CHEMISTRY OF MATERIALS

ARTICLE

pubs.acs.org/cm

Evaluation of Tavorite-Structured Cathode Materials for Lithium-Ion Batteries Using High-Throughput Computing

Tim Mueller, Geoffroy Hautier, Anubhav Jain, and Gerbrand Ceder*

Massachusetts Institute of Technology, 77 Massachusetts Avenue 13-5051, Cambridge Massachusetts 02139, United States

Supporting Information

ABSTRACT: Cathode materials with structure similar to the mineral tavorite have shown promise for use in lithium-ion batteries, but this class of materials is relatively unexplored. We use high-throughput density-functional-theory calculations to evaluate tavorite-structured oxyphosphates, fluorophosphates, oxysulfates, and fluorosulfates for use as cathode materials in lithium-ion batteries. For each material we consider the insertion of both one and two lithium ions per redox-active metal, calculating average voltages and stability relative to a database of nearly 100,000 previously calculated compounds. To evaluate lithium mobility, we calculate the activation energies for lithium diffusion through the known tavorite cathode materials $LiVO(PO_4)$, $LiV(PO_4)F$, and $LiFe(SO_4)F$. Our calculations indicate that tavorite-structured materials are capable of very high rates of one-dimensional lithium diffusion, and several tavorite-structured materials may be capable of reversibly inserting two lithium ions per redox-active metal.

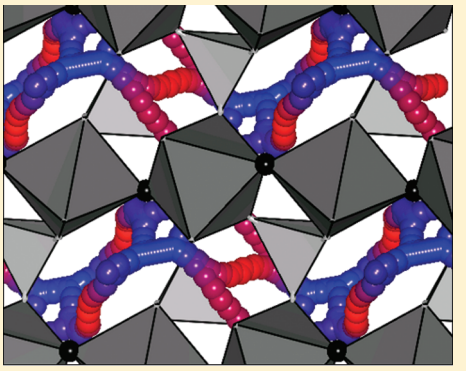

KEYWORDS: lithium-ion battery, cathode material, tavorite, density functional theory, high-throughput, computational

INTRODUCTION

In the search for better cathode materials for lithium-ion batteries, researchers have had considerable success developing and optimizing materials with spinel,[1] olivine,[2] or layered[3] structures. However to realize nonincremental improvements in battery capacity, reliability, and safety it may be necessary to develop cathode materials with different crystal structures. An ideal cathode material should combine thermal stability, high voltage, and high lithium mobility and capacity, but it is difficult to achieve these goals in one material. Materials containing polyatomic phosphate $(PO_4)^{3-}$ anions tend to have higher thermal stability than oxides with comparable voltages,[2,4−7] but these large and heavy anions adversely affect specific capacity. One way to compensate for this loss of capacity would be to develop a material that contains a polyatomic anion and is capable of reversibly inserting two lithium ions per redox-active metal ion. Recent studies indicate that materials with a structure similar to $LiFe(PO_4)(OH)$ (tavorite) might be able to achieve this goal.

Tavorite belongs to a class of materials with the general formula $AM(TO_4)X$, where A is typically an alkali or alkaline-earth element, M is a metal, T is a p-block element, and X is O, OH, or F. The structure consists of vertex-linked one-dimensional (1D) chains of MO_4X_2 octahedra connected by TO_4 tetrahedra. The X anions are located at the vertices shared by neighboring MO_4X_2 octahedra, and the A cations may be located at a number of sites throughout the framework (Figure 1). There are numerous minerals in this class, including $LiAl(PO_4)F$ (amblygonite) and $CaTiO(SiO_4)$ (titanite), but for clarity we will refer to materials in this class as tavorite-structured. Marx et al. have demonstrated reversible lithium insertion in $LiFe(PO_4)(OH)$ (tavorite) and tavorite-structured $Fe(SO_4)(H_2O)$,[8,9] and Reddy et al. have demonstrated reversible lithium insertion in $Fe(SO_4)(OH)$.[10] One of the first tavorite-structured materials considered for lithium-ion batteries was α-$LiVO(PO_4)$, which was shown to have a capacity of 126 mAh/g at 3.8 V.[11] Barker et al. demonstrated that the substitution of fluorine for oxygen to create tavorite-structured $LiV(PO_4)F$ increases the voltage to about 4.2 V and increases the rate capability of the material.[12,13] Their work on a symmetric $LiV(PO_4)F/LiV(PO_4)F$ cell also demonstrated that the tavorite structure can cycle lithium between compositions $M(TO_4)X$ and $Li_2M(TO_4)X$.[14] In addition, tavorite-structured $LiV(PO_4)F$ demonstrates exceptional thermal stability, exceeding that of olivine $LiFe(PO_4)$.[15,16] Following up on a report of good lithium-ion conductivity in tavorite-structured $LiMg(SO_4)F$,[17] Recham et al. recently demonstrated high-rate lithium insertion in tavorite-structured $LiFe(SO_4)F$.[18] In another paper, Recham et al. showed that it is possible to insert additional lithium into $LiTi(PO_4)F$, taking advantage of the Ti^{2+}/Ti^{3+} redox couple.[19] Ramesh et al. demonstrated that $LiFe(PO_4)F$ can incorporate two lithium ions per redox-active metal, as evidenced by reversible cycling between $LiFe(PO_4)F$ and $Li_2Fe(PO_4)F$.[20] These results suggest that given the right chemistry, it may be possible to find a tavorite-structured

Received: March 15, 2011
Revised: August 3, 2011
Published: August 17, 2011

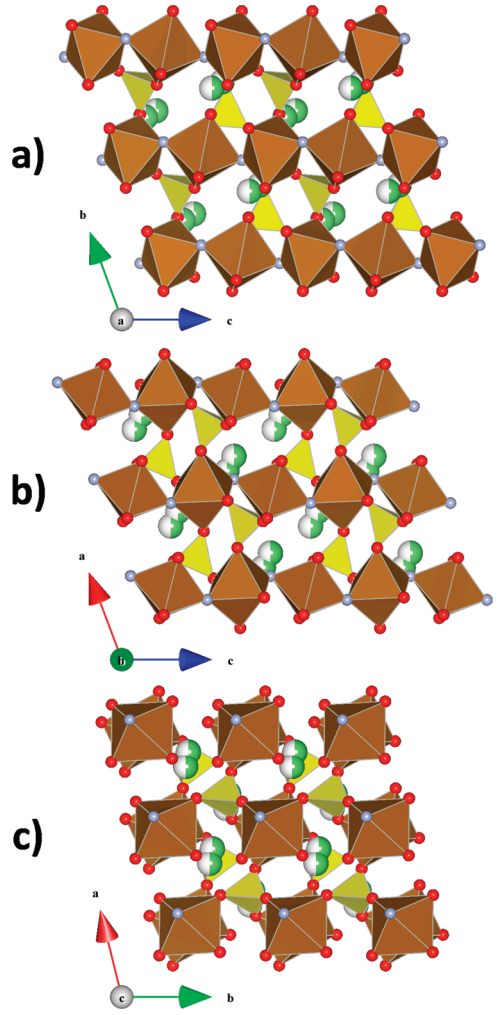

Figure 1. 2 × 2 × 2 supercell of a typical tavorite-structured material, LiFe(SO$_4$)F. Structural data is from ref 18. Brown octahedra represent Fe, yellow tetrahedra represent S, red spheres represent O, and blue spheres represent F. The green-and-white spheres represent partially occupied lithium sites, with the occupancy given by the fraction of the sphere shaded green. The three views are (a) along the *a* axis, (b) along the *b* axis, and (c) along the *c* axis.

electrode material with high capacity, excellent stability, and the ability to insert lithium at high rates.

In this paper we use high-throughput computing to search for promising tavorite-structured cathode materials. We substitute seventeen redox-active metals (Table 1) into tavorite-structured oxyphosphates, fluorophosphates, oxysulfates, and fluorosulfates, and for each host material we calculate the average voltages for insertion of both one and two lithium ions per metal ion. To screen out compounds that are unlikely to be sufficiently stable for use in batteries, we evaluate the stability of each candidate material against a database of nearly 100,000 materials for which we have calculated energies.[21] To better understand the rate capabilities of tavorite-structured materials, we model lithium diffusion through three well-known tavorite-structured compounds: VO(PO$_4$), V(PO$_4$)F, and Fe(SO$_4$)F. Our results highlight several promising chemistries, including a number that may be capable of inserting two lithium ions per redox-active metal.

Table 1. Redox-Active Metals Considered and the (U-J) Parameters Assigned to Them for GGA+U Calculations

metal	(U-J) value
Ag	1.5
Bi	0.0
Co	5.7
Cr	3.5
Cu	4.0
Fe	4.0
Mn	3.9
Mo	3.5
Nb	1.5
Ni	6.0
Pb	0.0
Sb	0.0
Sn	0.0
Ta	2.0
Ti	0.0
V	3.1
W	4.0

METHODS

The average voltage relative to lithium metal for lithium insertion into a host material *M* is given by

$$V(x) = \frac{G(\mathrm{M}) + xG(\mathrm{Li}) - G(\mathrm{Li}_x\mathrm{M})}{xz} \quad (1)$$

where *V* is the voltage, *G*( ) is the Gibbs free energy per formula unit, and *z* is the elementary charge per lithium ion (*z* = 1). Because the contribution of pressure and entropy to the free-energy differences is expected to be relatively small,[22] eq 1 is well-approximated by considering only energies:

$$V(x) = \frac{E(\mathrm{M}) + xE(\mathrm{Li}) - E(\mathrm{Li}_x\mathrm{M})}{xz} \quad (2)$$

where *E*( ) is the energy per formula unit. To calculate the energies in eq 2, we use spin-polarized density functional theory[23] (DFT) with the Perdew−Burke−Ernzerhof (PBE) exchange-correlation functional[24] as implemented in the Vienna Ab-initio Simulation Package (VASP).[25] To calculate accurate voltages for transition metal oxides,[26] we use the generalized gradient approximation with Hubbard U corrections (GGA+U) in the rotationally invariant form proposed by Dudarev et al.[27] The (U−J) parameters, provided in Table 1, were fit to empirical oxidation energies as described in ref 28. The only exception was cobalt, for which we found that a (U−J) value of 5.7, similar to the values found by Zhou et al.,[26] produces better results. A *k*-point density of 500 *k*-points per reciprocal atom was used for all calculations. All cells were allowed to fully relax, and precision for all calculations was set to "high", which increases the plane-wave cutoff energy by 25% above the VASP default. The electronic and ionic minimization convergence criteria were set to the VASP defaults of 1 meV per unit cell and 10 meV per unit cell, respectively. Initial magnetic moments were set to high-spin (MAGMOM = 5) for Ti, V, Cr, Mn, Fe, Co, Ni, Cu, Nb, Mo, Ag, Ta, and W, and low-spin (MAGMOM = 0.6) for the other elements. It was found that cobalt frequently does not relax to a low-spin ground state when initialized in a high-spin state, even if the low-spin state has lower energy. For this reason all Co-containing calculations were run twice, initialized in both high-spin and low-spin states, and the calculation resulting in the lowest energy was used. All voltage calculations were run both with both ferromagnetic and antiferromagnetic spin initialization,

and in all cases the result with lowest energy was used. VASP calculations were managed using the AFLOW/ACONVASP framework.[29]

We have compiled a database of nearly 100,000 structural energies calculated using these same parameters, with the following exceptions: In the database all calculations were initialized in a ferromagnetic spin state, the electronic minimization convergence criterion was set to 5×10^{-5} eV per atom, and the ionic minimization convergence criterion was set to 5×10^{-4} eV per atom. The settings used for the energies in the database are well-suited for high-throughput calculations, but they will typically result in slightly higher calculated energies than the settings used in this paper. In almost all cases the difference is less than 10 meV/atom. To assess the thermodynamic stability and oxygen chemical potential of each tavorite-structured compound in this paper, we compared the energy of each compound to a thermodynamic hull constructed from the compounds in our database according to the methodology outlined by Ong et al.[30] Stability for a given compound is evaluated against any linear combination of compounds in the database that have the same averaged composition. To evaluate thermodynamic stability against oxygen gas, we fit the oxygen chemical potential to experimental data as outlined by Wang et al.[31] and used a reference temperature of 298 K and a partial pressure of 1 atm.

Energies were calculated for all combinations of tavorite-structured compounds with the general formula Lix$M(TO_4)X$, where x is 0, 1, or 2; M is one of Ag, Bi, Co, Cr, Cu, Fe, Mn, Mo, Nb, Ni, Pb, Sb, Sn, Ta, Ti, V, or W; T is P or S; and X is O or F. Because the oxidation states Ag^{4+}, Ag^{5+}, Bi^{1+}, Bi^{2+}, Co^{5+}, Cr^{1+}, Cu^{4+}, Cu^{5+}, Fe^{5+}, Mo^{1+}, Nb^{1+}, Pb^{1+}, Pb^{5+}, Sb^{1+}, Sb^{2+}, Sn^{1+}, Sn^{5+}, Ta^{1+}, Ti^{1+}, V^{1+}, and W^{1+} have very rarely (or never) been observed, compounds that would require these oxidation states were excluded from the search. Compounds in which nearest neighbors for the M or T elements changed after structural relaxation were removed from consideration, as we are only interested in materials that insert lithium topotactically.

To determine the initial positions of the atoms in each of the compounds, the redox-active metals were substituted into template materials. These templates were used as the starting point for the structural relaxation in the calculations. For Li$M(SO_4)$F and Li$MO(SO_4)$ materials, the structural specification for LiFe(SO_4)F from ref 18 was used as a template, and for Li$M(PO_4)$F calculations, the structural specification for LiFe(PO_4)F from ref 20 was used as a template. For Li$M(SO_4)$F, Li$MO(SO_4)$, and Li$M(PO_4)$F, calculations were run with lithium atoms located both at site Li1 and site Li2 as specified in refs 18 and 20, and the lowest-energy result was used. For Li$MO(PO_4)$ calculations, the structural specification for LiV$O(PO_4)$ from ref 32 was used as a template. For all $M(TO_4)X$ calculations, the Li$M(TO_4)X$ template was used with the lithium removed. We are not aware of any available atomic-level structural data for $Li_2M(TO_4)X$ compounds. We have found two low-energy structures for $Li_2Fe(PO_4)F$ that agree well with the experimental voltages and lattice parameters provided in ref 20. The coordinates for these structures are provided in the Supporting Information. Both structures were used as templates for all $Li_2M(TO_4)X$ calculations, and for each material we use the result with the lowest calculated energy. The space group of each of the templates used is either $P1$ or $P\bar{1}$. Materials initialized with the $P\bar{1}$ space group may be unable to relax to a lower-energy structure that does not have inversion symmetry, which may lead to errors in the calculated energies. To test this, we re-relaxed all Mn- and Cu-containing compounds after randomly perturbing the initial positions of the atoms. In all cases the final relaxed energy changed by less than 10 meV per atom, suggesting that the constraint of inversion symmetry does not significantly affect the calculated energies.

The activation energy for diffusion was determined by a two-step process: first, a screened Coulomb potential with exponential repulsion was used to identify the topology of likely diffusion paths and generate a set of possible lithium hops. The activation energy for each hop was then calculated by density functional theory, using the nudged elastic band (NEB) method as implemented in VASP compiled with the VASP Transition State Tools.[33−35] For each NEB calculation, sufficient images were used to ensure that the initial lithium positions in successive images were no more than 0.5 Å from each other. All NEB calculations were initialized with a ferromagnetic spin state, and to avoid ambiguity regarding the localization of electrons, pure GGA (without the Hubbard U correction) was used. Tests on Fe(SO_4)F and V(PO_4)F indicated that these choices had little effect on the calculated activation energies. Each NEB calculation was performed on a supercell large enough to ensure that no lithium ion was within 8 Å from its periodic image, resulting in compositions of $Li_{1/10}V(PO_4)F$, $Li_{1/10}Fe(SO_4)F$, and $Li_{1/12}VO(PO_4)$. The volume was frozen at the volume of the relaxed delithiated structure, and only the k-point located at Γ (the Brillouin zone center) was used. Ions were relaxed using the global limited-memory Broyden−Fletcher−Goldfarb−Shannon method as implemented in the VASP Transition State Tools.[36,37] The network of hops was exhaustively searched to find the minimum-energy path from one lithium site to a transitionally equivalent site. To calculate the energy at the saddle point, cubic splines were fit through the images along each hop.

RESULTS

The calculated lithium insertion voltages and volume changes for the tavorite-structured fluorophosphates, fluorosulfates, oxyphosphates, and oxysulfates considered in this study are given in Table 2, Table 3, Table 4, and Table 5, respectively. Upon lithiation, the volume of LiFe(PO_4)F is predicted to increase by 8.0%, which is close to the 8.8% reported experimentally, suggesting that the template we have chosen for $Li_2M(TO_4)X$ compounds is realistic. Likewise, we predict insertion voltages for $Li_2Fe(PO_4)F$ and $Li_2V(PO_4)F$ that are consistent with experiments. A comparison between the calculated voltages and values reported in the literature for V(PO_4)F, V$O(PO_4)$, Fe(SO_4)F, LiFe(PO_4)F, and LiTi(PO_4)F is given in Table 6. Because the average voltage for LiFe(PO_4)F was not directly reported in ref 20, we used the data in that paper to estimate an average. The calculated values agree very well with the experimental values for all materials except V(PO_4)F and LiTi(PO_4)F. For $Li_xV(PO_4)F$ with $0 < x < 1$, we underestimate the voltage by about 0.4 eV, but we are close to the experimental value for $x > 1$. Another computational study using similar methods also underestimated the voltage of this material, although to a lesser extent.[38] For $Li_xTi(PO_4)F$ we predict significantly lower voltages than reported experimentally, especially for the uncommon Ti^{2+}/Ti^{3+} redox couple.[19] A similar underestimation of the voltage for titanium phosphates has previously been observed in calculations using the local density approximation.[39,40] For both Ti and V, the (U-J) value we used, which was calibrated to oxides, may not be the optimal value to calculate energies for oxyfluorides. This may be true for other early transition metals as well, implying that for these materials the voltages reported in this paper may be too low. On the other hand the voltages we calculate for lithium insertion in (Mn, Co, Ni)(SO_4)F are 4.27 V, 4.93 V, and 5.35 V, respectively, which are comparable to the "back-of-the-envelope" values of 4.25 V, 4.95 V, and 5.25 V derived in ref 41, as well as the voltages calculated using density functional theory in ref 42. Of these materials, tavorite-structured LiMn(SO_4)F has yet to be synthesized, and the Co- and Ni- containing structures show no redox activity up to 5 V.[41]

To screen out compounds that are unlikely to be stable, for each material we searched our database of materials to identify the decomposition reaction with the greatest decomposition energy. In our experience, any compound that releases more than

Table 2. Calculated Voltages and Volume Changes Relative to Li/Li^+ for Li Insertion into Fluorophosphate Host Materials[a]

host material ($M^{4+}X$)	voltage ($M^{4+}X \rightarrow LiM^{3+}X$)	voltage ($LiM^{3+}X \rightarrow Li_2M^{2+}X$)	voltage ($M^{4+}X \rightarrow Li_2M^{2+}X$)	ΔV ($M^{4+}X \rightarrow LiM^{3+}X$)	ΔV ($LiM^{3+}X \rightarrow Li_2M^{2+}X$)	screened Wh/kg	screened Wh/L
$Ag(PO_4)F$	N/A	4.34*	N/A	N/A	6%	493	1790
$Bi(PO_4)F$	4.59	N/A	N/A	3%	N/A	0	0
$Co(PO_4)F$	5.26	4.11*	4.68	2%	7%	589	1928
$Cr(PO_4)F$	4.89*	2.19*	3.54*	3%	13%	1054	3147
$Cu(PO_4)F$	N/A	4.54*	N/A	N/A	9%	635	2128
$Fe(PO_4)F$	5.14	2.92*	4.03	−3%	8%	426	1338
$Mn(PO_4)F$	4.86*	3.45*	4.15*	7%	10%	1218	3708
$Mo(PO_4)F$	3.33*	n.t.	n.t.	2%	n.t.	411	1501
$Nb(PO_4)F$	1.80	0.85	1.33	−1%	3%	0	0
$Ni(PO_4)F$	5.50	4.59*	5.04	−1%	3%	660	2216
$Pb(PO_4)F$	4.27*	3.69*	3.98*	8%	6%	636	3031
$Sb(PO_4)F$	3.25*	N/A	N/A	7%	N/A	359	1314
$Sn(PO_4)F$	2.68*	n.t.	n.t.	12%	n.t.	300	1127
$Ta(PO_4)F$	1.05	0.53	0.79	−4%	3%	0	0
$Ti(PO_4)F$	2.25*	0.54	1.39	2%	6%	357	1078
$V(PO_4)F$	3.80*	1.85*	2.83*	4%	8%	847	2564
$W(PO_4)F$	2.15*	n.t.	n.t.	1%	n.t.	189	961

[a] Steps in which both end-members pass our stability screen are marked with an asterisk and steps which are not topotactic labeled with "n.t.".

Table 3. Calculated Voltages and Volume Changes Relative to Li/Li^+ for Li Insertion into Fluorosulfate Host Materials[a]

host material ($M^{3+}X$)	voltage ($M^{3+}X \rightarrow LiM^{2+}X$)	voltage ($LiM^{2+}X \rightarrow Li_2M^{1+}X$)	voltage ($M^{3+}X \rightarrow Li_2M^{1+}X$)	ΔV ($M^{3+}X \rightarrow LiM^{2+}X$)	ΔV ($LiM^{2+}X \rightarrow Li_2M^{1+}X$)	screened Wh/kg	screened Wh/L
$Ag(SO_4)F$	4.98*	4.09*	4.54*	5%	6%	1027	3487
$Co(SO_4)F$	4.93*	0.89	2.91	7%	10%	730	2383
$Cr(SO_4)F$	2.95*	N/A	N/A	15%	N/A	455	1320
$Cu(SO_4)F$	5.09*	n.t.	n.t.	2%	n.t.	735	2447
$Fe(SO_4)F$	3.62*	0.15	1.88	7%	9%	545	1701
$Mn(SO_4)F$	4.27*	n.t.	n.t.	9%	n.t.	647	1923
$Mo(SO_4)F$	1.61	N/A	N/A	14%	N/A	0	0
$Nb(SO_4)F$	1.35	N/A	N/A	1%	N/A	0	0
$Ni(SO_4)F$	5.35*	n.t.	n.t.	0%	n.t.	794	2669
$Pb(SO_4)F$	4.46*	N/A	N/A	5%	N/A	363	1636
$Sn(SO_4)F$	2.99*	N/A	N/A	8%	N/A	333	1115
$Ta(SO_4)F$	0.88	N/A	N/A	−8%	N/A	0	0
$Ti(SO_4)F$	1.15	N/A	N/A	5%	N/A	0	0
$V(SO_4)F$	2.57*	N/A	N/A	7%	N/A	399	1187
$W(SO_4)F$	0.93	N/A	N/A	3%	N/A	0	0

[a] Steps in which both end-members pass our stability screen are marked with an asterisk and steps which are not topotactic labeled with "n.t.".

0.1 eV/atom in energy upon decomposition is unlikely to be stable enough for use in a commercial battery. This simple test, which all known commercial cathode materials pass, enables us to screen out a large number of the tavorite-structured candidates. In Tables 1−4 we have highlighted with an asterisk (*) the cells for which both end-members of the insertion reaction pass this test, and we provide the total specific energy and energy density for these steps relative to a metallic lithium anode. We emphasize that the materials highlighted with an asterisk are the least likely to be unstable, but this is not a guarantee of either stability or metastability. Many of these materials are predicted to decompose exothermically, although with a relatively small decomposition energy as is often found for highly metastable materials. In addition, it is possible that our database is missing some decomposition products, in which case we may be underestimating the decomposition energy of some compounds. Because adding additional entries to our database could not possibly decrease the decomposition energies, we find that the stability screen is most useful in eliminating candidates that are unlikely to be stable.

The decomposition energy can also be used to identify compounds that may be difficult to synthesize. We find that it is often difficult to directly synthesize compounds that are predicted to release more than 30 meV per atom upon decomposition. Tavorite-structured compounds that are predicted to release less than 30 meV per atom upon decomposition, and are hence most likely to be directly synthesizable, are $LiCo(PO_4)F$, $LiCr(PO_4)F$, $LiFe(PO_4)F$, $LiMn(PO_4)F$, $Mo(PO_4)F$,

Table 4. Calculated Voltages and Volume Changes Relative to Li/Li^+ for Li Insertion into Oxyphosphate Host Materials[a]

host material ($M^{5+}X$)	voltage ($M^{5+}X \rightarrow LiM^{4+}X$)	voltage ($LiM^{4+}X \rightarrow Li_2M^{3+}X$)	voltage ($M^{5+}X \rightarrow Li_2M^{3+}X$)	$\Delta V(M^{5+}X \rightarrow LiM^{4+}X)$	$\Delta V(LiM^{4+}X \rightarrow Li_2M^{3+}X)$	screened Wh/kg	screened Wh/L
$AgO(PO_4)$	N/A	n.t.	n.t.	N/A	n.t.	0	0
$BiO(PO_4)$	4.45	3.31	3.88	7%	6%	0	0
$CoO(PO_4)$	N/A	4.45	N/A	N/A	5%	0	0
$CrO(PO_4)$	4.53	3.34	3.93	−3%	6%	0	0
$CuO(PO_4)$	N/A	n.t.	n.t.	N/A	n.t.	0	0
$FeO(PO_4)$	N/A	3.98*	N/A	N/A	8%	590	1917
$MnO(PO_4)$	4.91	3.82*	4.37	1%	13%	570	1807
$MoO(PO_4)$	3.35*	2.06*	2.70*	1%	4%	657	2422
$NbO(PO_4)$	2.04*	0.82*	1.43*	−13%	12%	352	1270
$NiO(PO_4)$	5.27	4.30	4.78	0%	3%	0	0
$PbO(PO_4)$	N/A	3.33	N/A	N/A	10%	0	0
$SbO(PO_4)$	2.97*	n.t.	n.t.	13%	n.t.	332	1307
$SnO(PO_4)$	N/A	1.71	N/A	N/A	13%	0	0
$TaO(PO_4)$	1.30	0.30	0.80	2%	0%	0	0
$TiO(PO_4)$	N/A	1.25	N/A	N/A	6%	0	0
$VO(PO_4)$	3.81*	2.41	3.11	−1%	6%	605	1929
$WO(PO_4)$	2.33*	1.03*	1.68*	1%	4%	292	1500

[a] Steps in which both end-members pass our stability screen marked with an asterisk and steps which are not topotactic labeled with "n.t.".

Table 5. Calculated Voltages and Volume Changes Relative to Li/Li^+ for Li Insertion into Oxysulfate Host Materials[a]

host material ($M^{4+}X$)	voltage ($M^{4+}X \rightarrow LiM^{3+}X$)	voltage ($LiM^{3+}X \rightarrow Li_2M^{2+}X$)	voltage ($M^{4+}X \rightarrow Li_2M^{2+}X$)	$\Delta V(M^{4+}X \rightarrow LiM^{3+}X)$	$\Delta V(LiM^{3+}X \rightarrow Li_2M^{2+}X)$	screened Wh/kg	screened Wh/L
$AgO(SO_4)$	N/A	n.t.	n.t.	N/A	n.t.	0	0
$BiO(SO_4)$	3.79	N/A	N/A	4%	N/A	0	0
$CoO(SO_4)$	5.13*	n.t.	n.t.	3%	n.t.	772	2597
$CrO(SO_4)$	3.77	n.t.	n.t.	9%	n.t.	0	0
$CuO(SO_4)$	N/A	n.t.	n.t.	N/A	n.t.	0	0
$FeO(SO_4)$	4.68	n.t.	n.t.	6%	N/A	0	0
$MnO(SO_4)$	4.54	n.t.	n.t.	4%	n.t.	0	0
$MoO(SO_4)$	2.27	n.t.	n.t.	4%	n.t.	0	0
$NbO(SO_4)$	1.29	n.t.	n.t.	3%	n.t.	0	0
$NiO(SO_4)$	5.01	n.t.	n.t.	3%	n.t.	0	0
$PbO(SO_4)$	4.18	n.t.	n.t.	12%	n.t.	0	0
$SbO(SO_4)$	2.85	N/A	N/A	8%	N/A	0	0
$SnO(SO_4)$	2.65	n.t.	n.t.	16%	n.t.	0	0
$TaO(SO_4)$	0.66	n.t.	n.t.	2%	n.t.	0	0
$TiO(SO_4)$	2.07	0.00	1.04	4%	6%	0	0
$VO(SO_4)$	3.02*	0.99	2.01	7%	9%	477	1468
$WO(SO_4)$	1.29	n.t.	n.t.	4%	n.t.	0	0

[a] Steps in which both end-members pass our stability screen marked with an asterisk and steps that are not topotactic labeled with "n.t.".

$LiMo(PO_4)F$, $Sn(PO_4)F$, $Ti(PO_4)F$, $V(PO_4)F$, $LiV(PO_4)F$, $W(PO_4)F$, $LiAg(SO_4)F$, $Li_2Ag(SO_4)F$, $Bi(SO_4)F$, $LiCo(SO_4)F$, $Cr(SO_4)F$, $LiCr(SO_4)F$, $LiCu(SO_4)F$, $Fe(SO_4)F$, $LiFe(SO_4)F$, $Mn(SO_4)F$, $LiMn(SO_4)F$, $Mo(SO_4)F$, $LiNi(SO_4)F$, $Pb(SO_4)F$, $Sb(SO_4)F$, $Sn(SO_4)F$, $V(SO_4)F$, $MoO(PO_4)$, $LiMoO(PO_4)$, $NbO(PO_4)$, $SbO(PO_4)$, $LiSnO(PO_4)$, $LiTiO(PO_4)$, $VO(PO_4)$, $LiVO(PO_4)$, $WO(PO_4)$, $CoO(SO_4)$, $LiCoO(SO_4)$, $MoO(SO_4)$, $SnO(SO_4)$, and $VO(SO_4)$.

We have found that the calculated oxygen chemical potential at which O_2 is released is a good proxy for the safety of a cathode material at high temperatures.[43,44] To evaluate the safety of the materials considered in this paper, we have calculated the oxygen chemical potentials of each material in the fully delithiated state. The materials that pass the thermodynamic stability screen, are not predicted to release oxygen at room temperature, and are predicted to insert lithium at more than 1 V relative to lithium metal are shown in Figure 2. By these metrics, the known tavorite cathode materials $VO(PO_4)$, $V(PO_4)F$, and $Fe(SO_4)F$ are among the safest and most stable tavorite-structured materials that insert lithium at more than 3 V relative to lithium metal. Materials with similar values for voltage, oxygen chemical potential, and thermodynamic stability include $Mo(PO_4)F$ and $MoO(PO_4)$.

dx.doi.org/10.1021/cm200753g |Chem. Mater. 2011, 23, 3854–3862

Table 6. Comparison between Calculated Voltages and Values from the Literature

delithiated state	lithiated state	calculated voltage	literature value	method	reference
$VO(PO_4)$	$LiVO(PO_4)$	3.81	3.8	experiment	11
$V(PO_4)F$	$LiV(PO_4)F$	3.80	4.2	experiment	12,14
			3.94	DFT (GGA + U)	38
$LiV(PO_4)F$	$Li_2V(PO_4)F$	1.85	1.8	experiment	14
$LiFe(PO_4)F$	$Li_2Fe(PO_4)F$	2.92	2.9	experiment	20
$Li_{1-x}Ti(PO_4)F$	$LiTi(PO_4)F$	2.25	2.9	experiment	19
$LiTi(PO_4)F$	$Li_{1+x}Ti(PO_4)F$	0.54	1.7	experiment	19
$Co(SO_4)F$	$LiCo(SO_4)F$	4.93	4.9	DFT (GGA + U)	42
$Fe(SO_4)F$	$LiFe(SO_4)F$	3.62	3.6	DFT (GGA + U)	42
			3.7	DFT (GGA + U)	46
			3.6	experiment	18
			3.69	DFT (GGA + U)	45
			3.54	DFT (HSE06)	58
$Ni(SO_4)F$	$LiNi(SO_4)F$	5.35	5.4	DFT (GGA + U)	42

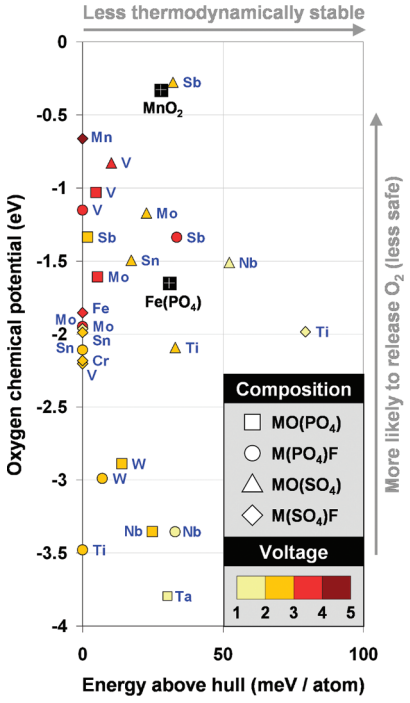

Figure 2. Energy relative to the thermodynamic hull and oxygen chemical potential for fully delithiated materials. The plotted materials pass our thermodynamic stability screen, are not predicted to release O_2 at room temperature, and are predicted to insert lithium at more than 1 V relative to lithium metal. The chemical composition is indicated by the shape of the symbol, with the redox-active metal labeled at the individual data points. The colors indicate the voltage at which lithium is predicted to be inserted relative to lithium metal. For reference, spinel MnO_2 and olivine $FePO_4$ have been added to the plot.

The experimentally resolved structures of $LiFe(PO_4)F$ and $LiFe(SO_4)F$ each contain two partially occupied symmetrically distinct lithium sites that are within 1 Å of each other.[18,20] In almost all of the $LiM(PO_4)F$, $LiM(SO_4)F$, and $LiMO(SO_4)$ materials that used these structures as templates, the structures with lowest energy contain lithium in Li1 sites. Exceptions are $LiCoO(SO_4)$, $LiCrO(SO_4)$, $LiFeO(SO_4)$, $LiVO(SO_4)$, $LiAg(SO_4)F$, $LiCr(SO_4)F$, $LiCu(SO_4)F$, $LiMo(SO_4)F$, and $LiW(SO_4)F$. This is in contrast to the computational results of Marx et al. and Ramzan et al., who find the Li2 site to have lower energy for $LiFe(PO_4)F$ and $LiFe(SO_4)F$, respectively.[9,45] We calculate the energy per lithium in the Li2 site to be higher than the energy per lithium in the Li1 site by 33 and 23 meV for $LiFe(PO_4)F$ and $LiFe(SO_4)F$, respectively. These discrepancies could be due to differences in computational parameters.

To evaluate lithium diffusion through tavorite-structured materials, we calculated the activation energies for diffusion in the dilute limit along all diffusion paths through $V(PO_4)F$, $Fe(SO_4)F$, and $VO(PO_4)$. Using the coordinate system of the $LiFe(SO_4)F$ structural data provided in ref 18, we find the lowest activation energy in all three structures is along the [111] direction (Figure 3). Because both site Li1 and site Li2 are either on or very close to this path, the diffusion path is unlikely to depend on which site lithium occupies. This appears to be the same path found by Liu and Huang,[46] and the activation energy we calculated (0.208 eV) is similar to the migration energy (0.3 eV) they calculated. However, Liu and Huang calculate the activation energy for diffusion as a sum of the migration energy and half of the lithium vacancy formation energy.[46] We do not believe that this approach is justified, as vacancies are created by electrochemical delithiation. Only for thermally controlled vacancy concentrations would the vacancy formation energy contribute to the activation energy for diffusion. Hence, it is sufficient to treat the "migration energy" as the activation energy.

We predict that in all three tavorite-structured materials diffusion occurs primarily along isolated channels. The calculated diffusion barriers for hops between channels are at least 250 meV higher than the diffusion barriers for transport along the channels, effectively making these materials 1D diffusers. Adams and Rao have used a force-field method to arrive at a similar result,[47] but Tripathi et al. have used a potential model to predict that $LiFe(SO_4)F$ is effectively a three-dimensional (3D) lithium-ion conductor.[48] We believe the differences in these results are due to the different energy models used, and that the density functional theory results presented in this paper are the most accurate. The activation energies to enable lithium diffusion in one, two, and three dimensions are given in Table 7, and the lowest-energy diffusion paths in three dimensions are shown in Figure 3. An input file for visualizing these paths using the VESTA[49] software

dx.doi.org/10.1021/cm200753g |*Chem. Mater.* 2011, 23, 3854–3862

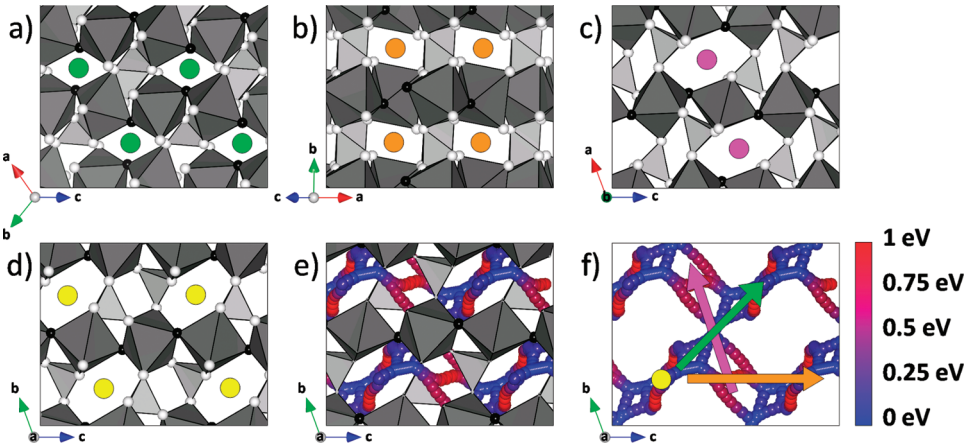

Figure 3. Lithium diffusion paths through a 2 × 2 × 2 supercell of $Fe(SO_4)F$. The paths through $V(PO_4)F$ and $VO(PO_4)$ are similar. Dark gray octahedra represent iron, light gray tetrahedra represent sulfur, white spheres represent oxygen, and black spheres represent fluorine. For clarity, oxygen ions located at the vertices of the tetrahedra are not shown in (e) and (f). (a) The green circles mark diffusion channels in the [111] direction, with an activation barrier of 208 meV. (b) The orange circles mark diffusion channels in the [101] direction, with an activation barrier of 700 meV. (c) The pink circles mark diffusion channels in the [010] direction with an activation barrier of 700 meV. (d) The yellow circles mark diffusion channels in the [100] direction, with an activation barrier of 976 meV. (e) The colored spheres represent all lithium diffusion paths with activation barriers below 1 eV, with the color indicating the energy difference between a point on the path and the lowest-energy lithium site. (f) The view shown in (e), with the host structure removed and the diffusion paths shown in (a), (b), and (c) indicated by color. A file for viewing these paths in VESTA[49] is included in the Supporting Information.

package are provided in the Supporting Information. Under the assumption that the rate of diffusion follows the Arrhenius equation, at room temperature 1D diffusion is predicted to be faster than two-dimensional (2D) diffusion by a factor that ranges from approximately 4×10^4 (for $VOPO_4$) to 2×10^8 (for $FeSO_4F$).

A rough estimate of diffusion coefficients can be derived from these activation energies using transition-state theory, in which the diffusion coefficient D in the dilute limit is given by

$$D = a^2 \nu e^{-E_a/kT} \quad (3)$$

where a is the length of a diffusion jump, ν is the attempt frequency, and E_a is the activation energy, and kT is Boltzmann's constant times the temperature.[50,51] A reasonable approximation for ν is 10^{12} Hz, roughly a typical phonon frequency.[50,52] From eq 3, the room-temperature diffusion coefficients for $VO(PO_4)$, $V(PO_4)F$, and $Fe(SO_4)F$ in the dilute limit are estimated to be 1×10^{-11}, 2×10^{-9}, and 2×10^{-7} cm^2/s respectively. We stress that these are diffusion coefficients for diffusion along the 1D channels, which requires unblocked channels.[53] Any channel blocking or defects may require activation of the 2D or 3D diffusion mechanisms.

DISCUSSION

Of the tavorite-structured materials considered in this paper, the fluorine-containing compounds are generally more stable than those without fluorine, and the phosphates are in general more stable than the sulfates. The stability of the fluorophosphates combined with the low activation energy for lithium diffusion in $V(PO_4)F$ (Table 7) suggests that fluorophosphates might hold the most promise as high-rate cathode materials. Fluorosulfates are similarly promising, although it is unlikely that any fluorosulfate can accommodate two lithium ions per redox-active metal. This is to be expected, as it would require the redox-active metal be reduced to a +1 oxidation state.

Table 7. Calculated Activation Energies for 1D, 2D, and 3D Lithium Diffusion in the Dilute Limit

	activation energy		
host material	1D	2D	3D
$VO(PO_4)$	463 meV	738 meV	1215 meV
$V(PO_4)F$	328 meV	803 meV	832 meV
$Fe(SO_4)F$	208 meV	700 meV	976 meV

On the basis of both the thermodynamic stability screen and the chemical potential at which oxygen release is predicted to occur, the materials most likely to be able to reversibly insert two lithium ions per redox-active metal are $V(PO_4)F$, $MoO(PO_4)$, $WO(PO_4)$, and $NbO(PO_4)$. This prediction is consistent with experimental results for $V(PO_4)F$.[14] These materials contain early transition metals, which are often able to exchange more than one electron without significantly destabilizing the material. Materials containing redox-active early transition metals tend to have lower average voltages than state-of-the-art cathode materials, but in the four materials listed above, this lower voltage is somewhat offset by higher theoretical gravimetric and volumetric capacities (Table 2, Table 4). The energy density and specific energies of these materials may be underestimated, as we have already noted that we predict a lower voltage than is experimentally observed for some tavorite-structured materials containing early transition metals. In each of these materials we predict a voltage step of at least 1 V, which may make it difficult to realize their full capacity in lithium-ion batteries.

Several of the chemistries considered in this paper both pass the thermodynamic stability screen and are relatively "safe", as measured by the oxygen chemical potential in the fully delithiated state (Figure 2). Of particular note is $MoO(PO_4)$, a material that could insert two lithium ions per redox-active metal based on our stability screen. $MoO(PO_4)$ has an oxygen chemical

dx.doi.org/10.1021/cm200753g |*Chem. Mater.* 2011, 23, 3854–3862

potential similar to that of $LiFe(PO_4)$, one of the safest known commercial cathode materials.

The calculated activation energy for 1D diffusion in $Fe(SO_4)F$ (208 meV) is significantly lower than the experimentally determined activation energy of ~990 meV for lithium insertion.[18] There are a number of possible explanations for this discrepancy. We have calculated the activation energies for lithium diffusion in the dilute limit (i.e., through $FeSO_4F$), whereas experiments were conducted on $LiFe(SO_4)F$.[18] It is possible that structural changes upon lithiation or lithium−lithium interactions account for some of the difference between the calculated and measured value. To investigate this possibility, we calculated the activation energy for vacancy diffusion along the minimum-energy path in $LiFe(SO_4)F$. The activation energy for vacancy diffusion through $LiFe(SO_4)F$ is calculated to be 44 meV lower than the activation energy for Li diffusion in $Fe(SO_4)F$. A similar result, showing little difference between the activation energy for lithium diffusion in the lithiated and delithiated state, was previously obtained for $LiFe(PO_4)$ and $Fe(PO_4)$.[52] These results suggest that the composition dependence of the activation energy is not sufficient to explain the apparent difference between theory and experiment.

Another possible explanation for the discrepancy between the experimental and theoretical activation energies is that defects in the host material may block the 1D low-energy path, and the rate-determining step may involve lithium diffusion around these defects. The fact that the calculated activation energy for 2D diffusion (700 meV) is much closer to the experimental activation energies is consistent with this explanation. A similar mechanism has recently been proposed to explain why experimentally measured lithium diffusion in large $LiFe(PO_4)$ particles is slower and more anisotropic than theoretically predicted.[52−55] In contrast to large particles, in small $LiFe(PO_4)$ particles in which it may be possible to transverse the entire length of the 1D diffusion pathway without encountering a defect, experimental evidence indicates that lithium diffusion is very fast.[56,57] It is possible that similar size-dependent diffusivity might be observed in tavorite-structured compounds. Because the calculated 1D activation energy for diffusion in $Fe(SO_4)F$ is close to that of $Fe(PO_4)$,[52] the very high rates seen in small $Fe(PO_4)$ particles might also be obtained in small, low-defect $Fe(SO_4)F$ particles.

Since it is unlikely that in large particles of $LiFe(SO_4)F$ the channels are completely defect-free, the good rate capability observed in this compound[18] can not solely be attributed to the low activation energy for lithium diffusion in the channels. Therefore a reasonable mechanism for crossover between the channels is required. Crossover can occur through the 2D or 3D hop mechanisms that we identified in the perfect structure (Figure 3). If one considers that a crossover jump is the critical activated process, then the effective diffusion rate will be roughly proportional to $a^2 e^{(-E_a/kT)}$, where E_a is the activation barrier for hops between channels and a is the distance between channel-blocking defects. Thus if lithium migration around channel-blocking defects is the rate-limiting step, there may be both a larger prefactor and a higher activation energy for diffusivity than there would be in a perfect crystal. It is also possible that channel-blocking defects may facilitate the transfer of lithium between channels by lowering the activation energy for lithium movement between channels, as has been predicted in $LiFe(PO_4)$.[52,53]

There are two wide channels in tavorite-structured materials (Figure 3c and Figure 3d) that are not quite symmetrically equivalent because of minor rotations in the octahedral and tetrahedral groups. Intuitively, it might seem that diffusion occurs readily through these channels, but we do not calculate this to be the case. The low-energy path for 1D diffusion is not along either of these channels. One of the channels contains the minimum-energy path that enables 2D diffusion, and the other contains the minimum-energy path that enables 3D diffusion. The relatively high activation energies for diffusion along these channels may be because passage through these channels requires the lithium ion to pass near the faces of two PO_4 or SO_4 tetrahedra, which results in large electrostatic repulsion with the P^{5+} or S^{6+} cations. In contrast, the low-energy path for 1D diffusion does not pass by the faces of any PO_4 or SO_4 tetrahedra.

Although the low-energy path does not pass by the faces of any PO_4 or SO_4 tetrahedra, it does pass between the faces of two MO_4X_2 octahedra. The activation energy for diffusion on the low-energy path is determined by the difference in energy between a low-energy site near an X anion and the high-energy saddle point that is face-sharing with two MO_4X_2 octahedra. Greater negative charge on the X anion decreases the electrostatic energy of the low-energy site, and greater positive charge on the M cations increases the energy of the saddle point. Thus we can expect diffusion to be fastest when the X anion has an oxidation state of −1, and the M cation has a low oxidation state. This is consistent with our calculated data (Table 7). The fluorides have the lowest activation energies for diffusion, and the diffusion barriers (463, 328, and 208 meV) decrease as the oxidation states on the respective M cations decrease (+5, +4, and +3). In general, we expect that this correlation between oxidation states close to zero and low diffusion barriers may be observed in a variety of materials, as it leads to a flatter electrostatic potential energy surface.

CONCLUSIONS

We have used high-throughput calculations to evaluate 64 different tavorite-structured cathode materials for lithium-ion batteries. Of these, we have identified four chemistries that we believe are most likely to be able to reversibly insert two lithium-ions per redox-active metal, resulting in capacities up to 300 mAh/g. Our calculations indicate that based on stability and diffusion barriers, the fluorosulfate and fluorophosphate families of materials are the most promising, and the oxysulfate family is the least. In addition, we have calculated activation energies for lithium diffusion through the known tavorite-structured cathode materials $Fe(PO_4)F$, $VO(PO_4)$, and $V(PO_4)F$. We predict that tavorite-structured materials have 1D diffusion channels with low activation energies that might enable charge and discharge of $Fe(SO_4)F$ and $V(PO_4)F$ at very high rates comparable to those observed in small olivine $Fe(PO_4)$ particles. These results suggest that tavorite-structured cathode materials are leading candidates to enable the next generation of lithium-ion batteries.

ASSOCIATED CONTENT

Supporting Information. Includes structural information for the two $Li_2M(TO_4)X$ templates and a VESTA[49] file for viewing diffusion paths. This material is available free of charge via the Internet at http://pubs.acs.org.

AUTHOR INFORMATION

Corresponding Author
*E-mail: gceder@mit.edu.

■ ACKNOWLEDGMENT

We thank Charles Moore for conversations regarding diffusion calculations. Figures in this paper were generated using VESTA.[49] This work was funded by Umicore N.V. and Robert Bosch GmbH. This work was supported in part by the MRSEC Program of the National Science Foundation under award number DMR-0819762.

■ REFERENCES

(1) Thackeray, M. M.; David, W. I. F.; Bruce, P. G.; Goodenough, J. B. *Mater. Res. Bull.* **1983**, *18*, 461–472.
(2) Padhi, A. K.; Nanjundaswamy, K. S.; Goodenough, J. B. *J. Electrochem. Soc.* **1997**, *144*, 1188.
(3) Mizushuma, K.; Jones, P. C.; Wiseman, P. J.; Goodenough, J. B. *Solid State Ionics* **1981**, *3/4*, 171–174.
(4) Jiang, J.; Dahn, J. R. *Electrochem. Commun.* **2004**, *6* (1), 39–43.
(5) Takahashi, M.; Tobishima, S.; Takei, K.; Sakurai, Y. *Solid State Ionics* **2002**, *148* (3−4), 283–289.
(6) Saidi, M. Y.; Barker, J.; Huang, H.; Swoyer, J. L.; Adamson, G. *J. Power Sources* **2003**, *119*, 266–272.
(7) Hautier, G.; Jain, A.; Ong, S. P.; Kang, B.; Moore, C.; Doe, R.; Ceder, G. *Chem. Mater.* **2011**, *23* (15), 3495−3508.
(8) Marx, N.; Croguennec, L.; Carlier, D.; Bourgeois, L.; Kubiak, P.; Le Cras, F.; Delmas, C. *Chem. Mater.* **2010**, *22* (5), 1854–1861.
(9) Marx, N.; Croguennec, L.; Carlier, D.; Wattiaux, A.; Le Cras, F.; Suard, E.; Delmas, C. *Dalton Trans.* **2010**, *39* (21), 5108–5116.
(10) Reddy, M. A.; Pralong, V.; Caignaert, V.; Varadaraju, U. V.; Raveau, B. *Electrochem. Commun.* **2009**, *11* (9), 1807–1810.
(11) Kerr, T. A.; Gaubicher, J.; Nazar, L. F. *Electrochem. Solid State Lett.* **2000**, *3* (10), 460–462.
(12) Barker, J.; Saidi, M. Y.; Swoyer, J. L. *J. Electrochem. Soc.* **2003**, *150* (10), A1394–A1398.
(13) Barker, J.; Gover, R. K. B.; Burns, P.; Bryan, A.; Saidi, M. Y.; Swoyer, J. L. *J. Power Sources* **2005**, *146* (1−2), 516–520.
(14) Barker, J.; Gover, R. K. B.; Burns, P.; Bryan, A. *Electrochem. Solid State Lett.* **2005**, *8* (6), A285–A287.
(15) Gover, R. K. B.; Burns, P.; Bryan, A.; Saidi, M. Y.; Swoyer, J. L.; Barker, J. *Solid State Ionics* **2006**, *177* (26−32), 2635–2638.
(16) Zhou, F.; Zhao, X. M.; Dahn, J. R. *Electrochem. Commun.* **2009**, *11* (3), 589–591.
(17) Sebastian, L.; Gopalakrishnan, J.; Piffard, Y. *J. Mater. Chem.* **2002**, *12* (2), 374–377.
(18) Recham, N.; Chotard, J. N.; Dupont, L.; Delacourt, C.; Walker, W.; Armand, M.; Tarascon, J. M. *Nat. Mater.* **2010**, *9* (1), 68–74.
(19) Recham, N.; Chotard, J. N.; Jumas, J. C.; Laffont, L.; Armand, M.; Tarascon, J. M. *Chem. Mater.* **2010**, *22* (3), 1142–1148.
(20) Ramesh, T. N.; Lee, K. T.; Ellis, B. L.; Nazar, L. F. *Electrochem. Solid State Lett.* **2010**, *13* (4), A43–A47.
(21) Jain, A.; Hautier, G.; Moore, C. J.; Ping Ong, S.; Fischer, C. C.; Mueller, T.; Persson, K. A.; Ceder, G. *Comput. Mater. Sci.* **2011**, *50* (8), 2295–2310.
(22) Aydinol, M. K.; Kohan, A. F.; Ceder, G. *J. Power Sources* **1997**, *68*, 664–668.
(23) Hohenberg, P.; Kohn, W. *Phys. Rev.* **1964**, *136*, 864.
(24) Perdew, J. P.; Burke, K.; Ernzerhof, M. *Phys. Rev. Lett.* **1996**, *77* (18), 3865–3868.
(25) Kresse, G.; Furthmuller, J. *Phys. Rev. B* **1996**, *54*, 11169.
(26) Zhou, F.; Cococcioni, M.; Marianetti, C. A.; Morgan, D.; Ceder, G. *Phys. Rev. B* **2004**, *70*, 23.
(27) Dudarev, S. L.; Botton, G. A.; Savrasov, S. Y.; Humphreys, C. J.; Sutton, A. P. *Phys. Rev. B* **1998**, *57* (3), 1505–1509.
(28) Wang, L.; Maxisch, T.; Ceder, G. *Phys. Rev. B* **2006**, *73*, 19.
(29) Setyawan, W.; Curtarolo, S. *Comput. Mater. Sci.* **2010**, *49* (2), 299–312.
(30) Ong, S. P.; Wang, L.; Kang, B.; Ceder, G. *Chem. Mater.* **2008**, *20* (5), 1798–1807.
(31) Wang, L.; Maxisch, T.; Ceder, G. *Chem. Mater.* **2007**, *19* (3), 543–552.
(32) Lavrov, A. V.; Nikolaev, V. P.; Sadikov, G. G.; Poraikoshits, M. A. *Doklady Akademii Nauk. SSSR* **1982**, *266* (2), 343–346.
(33) Mills, G.; Jonsson, H.; Schenter, G. *Surf. Sci.* **1995**, *324*, 305–337.
(34) Jonsson, H.; Mills, G.; Jacobsen, K. W. Nudged Elastic Band Method for Finding Minimum Energy Paths of Transitions. In *Classical and Quantum Dynamics in Condensed Phase Simulations*; Berne, B. J., Ciccotti, G., Coker, D. F., Eds.; World Scientific Publishing Co.: Singapore, 1998.
(35) Henkelman, G.; Jonsson, H. *J. Chem. Phys.* **2000**, *113* (22), 9978–9985.
(36) Nocedal, J. *Math. Comput.* **1980**, *35* (151), 773–782.
(37) Sheppard, D.; Terrell, R.; Henkelman, G. *J. Chem. Phys.* **2008**, *128*, 13.
(38) de Dompablo, M.; Amador, U.; Tarascon, J. M. *J. Power Sources* **2007**, *174* (2), 1251–1257.
(39) Morgan, D.; Ceder, G.; Saïdi, M. Y.; Barker; Swoyer, J.; Huang, H.; Adamson, G. *Chem. Mater.* **2002**, *14*, 4684–4693.
(40) Kohn, W.; Sham, L. J. *Phys. Rev.* **1965**, *140*, A1133–A1138.
(41) Barpanda, P.; Recham, N.; Chotard, J. N.; Djellab, K.; Walker, W.; Armand, M.; Tarascon, J. M. *J. Mater. Chem.* **2010**, *20* (9), 1659–1668.
(42) Frayret, C.; Villesuzanne, A.; Spaldin, N.; Bousquet, E.; Chotard, J. N.; Recham, N.; Tarascon, J. M. *Phys. Chem. Chem. Phys.* **2010**, *12* (47), 15512–15522.
(43) Ceder, G. *MRS Bulletin* **2010**, *35* (9), 693–701.
(44) Ong, S. P.; Jain, A.; Hautier, G.; Kang, B.; Ceder, G. *Electrochem. Commun.* **2010**, *12* (3), 427–430.
(45) Ramzan, M.; Lebegue, S.; Ahuja, R. *Phys. Rev. B* **2010**, *82*, 12.
(46) Liu, Z. J.; Huang, X. J. *Solid State Ionics* **2010**, *181* (25−26), 1209–1213.
(47) Adams, S.; Rao, R. P. *Solid State Ionics* **2011**, *184* (1), 57–61.
(48) Tripathi, R.; Gardiner, G. R.; Islam, M. S.; Nazar, L. F. *Chem. Mater.* **2011**, *23* (8), 2278–2284.
(49) Momma, K.; Izumi, F. *J. Appl. Crystallogr.* **2008**, *41*, 653–658.
(50) Vineyard, G. H. *J. Phys. Chem. Solids* **1957**, *3* (1−2), 121–127.
(51) Kutner, R. *Phys. Lett. A* **1981**, *81* (4), 239–240.
(52) Morgan, D.; Van der Ven, A.; Ceder, G. *Electrochem. Solid State Lett.* **2004**, *7* (2), A30–A32.
(53) Malik, R.; Burch, D.; Bazant, M.; Ceder, G. *Nano Lett.* **2010**, *10* (10), 4123–4127.
(54) Amin, R.; Balaya, P.; Maier, J. *Electrochem. Solid State Lett.* **2007**, *10* (1), A13–A16.
(55) Prosini, P. P.; Lisi, M.; Zane, D.; Pasquali, M. *Solid State Ionics* **2002**, *148* (1−2), 45–51.
(56) Yamada, A.; Yonemura, M.; Takei, Y.; Sonoyama, N.; Kanno, R. *Electrochem. Solid State Lett.* **2005**, *8* (1), A55–A58.
(57) Kang, B.; Ceder, G. *Nature* **2009**, *458* (7235), 190–193.
(58) Ramzan, M.; Lebegue, S.; Kang, T. W.; Ahuja, R. *J. Phys. Chem. C* **2011**, *115* (5), 2600–2603.